SPE-185851-MS

Compaction and Dilation Effects on Polymer Flood Performance

D. Wang, University of North Dakota; R. S. Seright, New Mexico Tech; K. P. Moe Soe Let, K. Bhoendie, and W. R. Paidin, Staatsolie Maatschappij Suriname N.V.

This paper was prepared for presentation at the SPE Europec featured at 79th EAGE Conference and Exhibition held in Paris, France, 12–15 June 2017.

Abstract

During recent field applications of polymer flooding in unconsolidated reservoirs, questions have arisen concerning the role of compaction and/or dilation on flood performance. The primary goal for this paper was to assess the extent to which the compressible nature of a formation affects polymer flooding. The Tambaredjo field in Suriname (with in-situ oil viscosity ~600 cp) was used as a model for this study. Comparisons were made during simulations where formation compressibility was 5.6×10^{-4} psi^{-1} versus 1×10^{-6} psi^{-1}. During a simulated 17-year compaction drive with compressibility of 5.6×10^{-4} psi^{-1}, water cut gradually increased to average 20% (consistent with the actual field performance)—compared to 2% if compressibility was 1×10^{-6} psi^{-1}. Oil recovery during this period was 18% OOIP for the highcompressibility case versus 3% OOIP for the low-compressibility case. Subsequent to the above compaction drive, incremental oil recoveries from waterflooding and polymer flooding were significantly less (about half in our case) when compressibility was 5.6×10^{-4} psi^{-1} than when compressibility was 1×10^{-6} psi^{-1}—simply because the oil recovery target was less. For the many waterflooding and polymer flooding cases, most incremental oil was recovered within five years of starting injection—regardless of formation compressibility. Water cuts rose to high values within five years of injection, regardless of the viscosity of the injected fluid and the compressibility value. Consistent with the actual field application, the response to polymer injection varied greatly from well to well. However, our analysis indicated that these variations were due to existing heterogeneities within the pattern—not to the high compressibility of the formation. During simulation, polymer injection increased porosity by factors up to 1.5 and permeability by factors up to 2.3. Nevertheless, compaction or dilation had a fairly even (proportionate) effect on porosity and permeability throughout the pattern. If polymer injection was stopped after the simulated peak in porosity was reached (after 4-6 years of injection) and compaction was allowed to resume, a modest level of oil recovery resulted from this second compaction period (25%-38% of the incremental oil during polymer injection). However, substantially longer was required for the recovery (15-17 years versus 4-6 years for polymer flooding). Consequently, relying on re-compaction during this period of low oil prices may not be as profitable as one might hope. Our work suggests that there is an optimum rate, viscosity, and pressure for polymer flooding compressible formations. Flooding too rapidly results in pressures that waste much of the injection energy on dilating the formation—thereby detracting from efficient displacement of the oil.

These constraints restrict injection rate, viscosity, and pressure to a greater degree for very compressible formations than for incompressible formations.

Introduction

In most reservoirs, formation compressibility is sufficiently low ($1\text{-}8 \times 10^{-6}$ psi^{-1}) that compaction is not a major contributor to oil recovery. However, a compaction drive has been important in some reservoirs. Cook and Jewel (1996) reported compressibility up to 1.5×10^{-4} psi^{-1} for the chalk Valhall field in the North Sea —where over half of the oil production was attributed to compaction. Sulak (1991) and Sulak *et al.* (1991) reported compressibility of 0.5—1×10^{-4} psi^{-1} for the chalk Ekofisk field in the North Sea. The Wilmington field in southern California presents a well-known case where substantial surface subsidence was observed as a result of compaction during primary production (Mayuga 1970, Otott and Clarke 2007). In history matching the performance of the Wilmington field, Yang *et al.* (1998) used compressibility values ranging from 2.75×10^{-5} and 6×10^{-5} psi^{-1}. (Incidentally, Yang's paper was used as the basis for the current compaction model in the CMG STARS simulator.) Compaction/dilation phenomena are also thought to be important for polymer floods in Canada (Seright 2016).

Compaction played a major role during primary production of 20% OOIP from the Tambaredjo field in Suriname. In this field, a polymer flood pilot project was implemented, and an expansion of the polymer flood is under consideration (Moe Soe Let *et al.* 2012, Manichand *et al.* 2013, Manichand and Seright 2014, Delamaide *et al.* 2016). During simulations, a compressibility of 5.6×10^{-4} psi^{-1} was used to match reservoir behavior for this field. Individual production-well responses to the polymer flood varied greatly throughout the pilot project (Moe Soe Let *et al.* 2012, Delamaide *et al.* 2016). Most likely, reservoir heterogeneity was dominantly responsible for this variation. However, others factors could have contributed, including (1) the unconfined nature of the pilot project, (2) staged addition of two additional patterns to the original flood, (3) increases in injected polymer viscosity during the project, (4) the condition of the wells, and (5) the compressible nature of the formation. Our primary goal for this paper is to assess the extent to which the compressible nature of a formation affects polymer flooding. The Tambaredjo field is used as a model for this study. In view of current low oil prices, another goal of this work is to assess whether stopping polymer flooding and returning to a compaction drive has merit.

The Tambaredjo Reservoir and Polymer Pilot

Tambaredjo field is a shallow (300-425 m or 984-1394 ft) unconsolidated, thinly bedded, fluvial-deltaic Paleocene oil reservoir with low pressure sandstone. The reservoir contains 15°API heavy crude with produced oil viscosity averaging 1728 cp. Simulations of reservoir behavior suggested that in situ oil viscosity was ~600 cp. The proved area of the reservoir covers approximately 170 km^2 near the Atlantic Ocean in northern Suriname. Production began in 1982 and has grown to nearly 9,290 BOPD (as of December 2015) through drilling more than 1,000 wells. The field is characterized by a gentle northwarddipping monoclonal structure.

The target production formation, T-Unit, is located within the Lower Saramacca member of the Saramacca Formation in the stratigraphic column of the coastal plain of Suriname (Haskell *et al.* 2010). The formation is sedimentary and young geologically. The available evidence indicates that in the study area compaction is the dominate drive mechanism with a possibility of very weak water influx from the cretaceous Nickerie formation, located at the bottom of the T-Unit (Fig. 1).

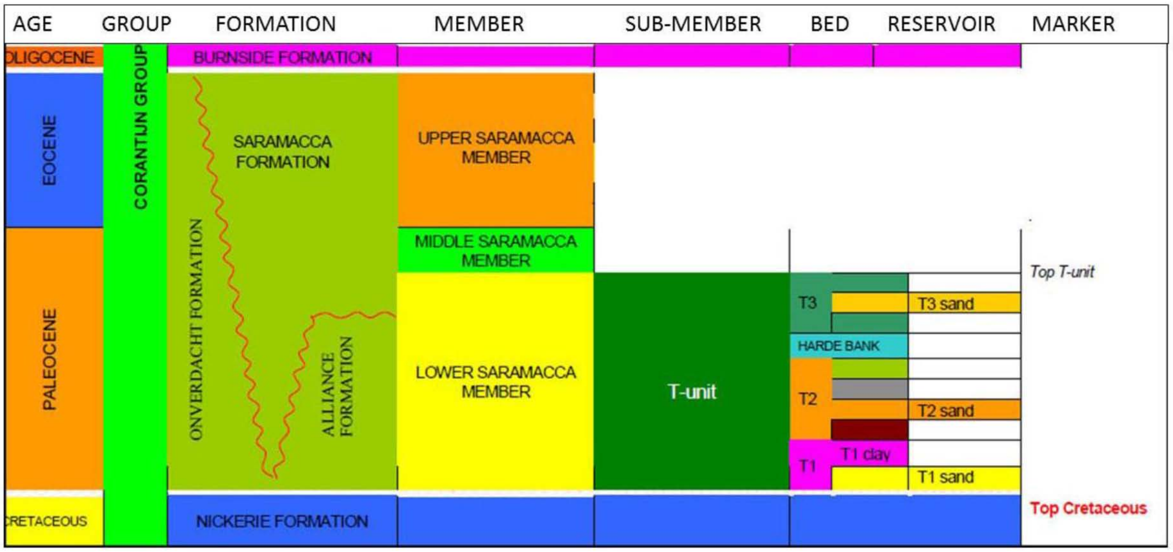

Figure 1—Stratigraphy column of the T-units (modified from Haskell *et al*. 2010)

A polymer flood was initiated in September 2008, where staged injection of 45-125-cp polymer solutions occurred in three contiguous patterns (Delamaide *et al.* 2016). As of mid-2016, 0.75 PV of polymer solution was injected, resulting in 11% OOIP incremental oil recovery over compaction. No waterflood was implemented prior to polymer flooding.

Numerical Simulation Model

Numerical models were established to simulate the mechanisms of compaction and dilation using field reservoir conditions and the Computer Modelling Group's (CMG) STARS simulator. Our model assumed constant compressibility and thermal expansion coefficient. In addition, the following assumptions were made:

- Elastic-plastic deformations via constant compressibility and thermal coefficient.
- Irreversible process of formation shrinkage due to pressure decline during primary depletion and rebound due to pressure rise during any subsequent injection period.
- The effect of compaction or rebound on fluid flow was simulated by the change of pore volume porosity.
- The pore volume compaction-rebound behavior was dominantly controlled by pressure.

During compaction and dilation, the relationship between grid block porosity, φ, and grid block pressure, p, was described by Eq. 1 (Beattie *et al.* 1991). Thermal expansion effects were not included because our system was isothermal. Fig. 2 depicts the process of compaction with elastic and plastic behavior for a sandstone reservoir.

$$\phi = \phi_{ref} e^{[C_p(p-p_{ref})]} \tag{1}$$

In the above equation, p_{ref} is a reference pressure, φ_{ref} is the porosity at p_{ref} and C_p is the pore volume compressibility. The simulator provides a set of quantities that characterize the deformation curves.

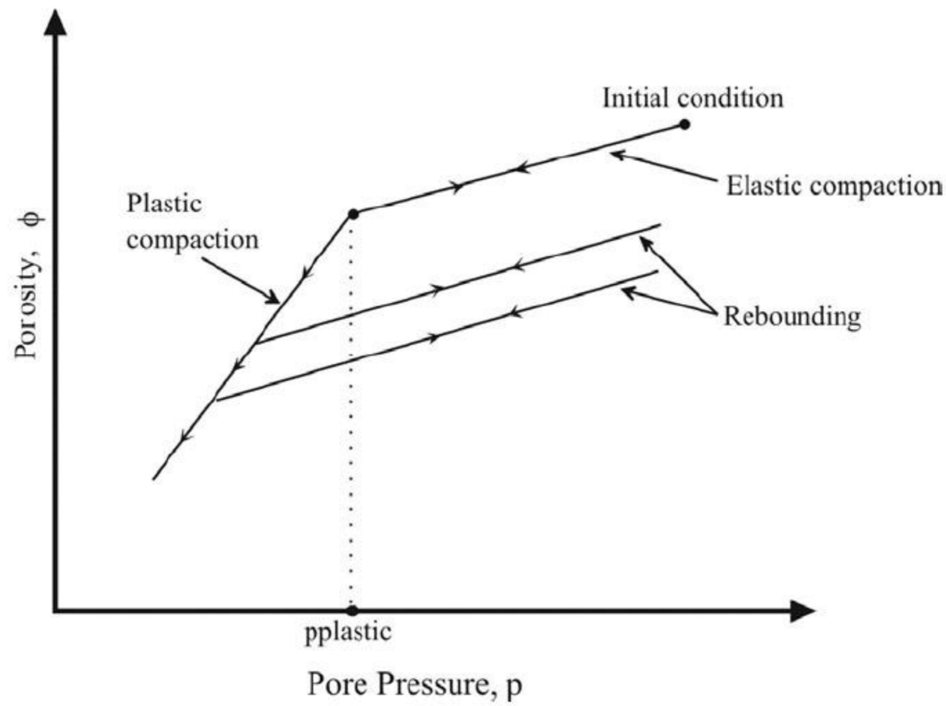

Figure 2—Rock compaction-rebounding model (CMG STARS Users Guide 2013)

Fig. 3 illustrates the simulation model that was built with 3-D heterogeneous grid blocks 15 × 15 × 1 in *x*, *y*, and *z* directions based on a well pattern from the Tambaredjo polymer flooding pilot project. For an average grid block in the T unit, *dx* = 28.804 m (94.5 ft), *dy* = 18.147 m (59.54 ft), *dz* = 10.88 m (35.71 ft). However, each grid block had a unique thickness in the *z*-direction. The average well spacing between injector and producer (in the simulation model) was 139.8 m (459 ft). A five-spot well pattern consisted of one injector (labeled I1 and corresponding to actual injector, 1M101), and four producers: P1, P2, P3, and P4—corresponding to actual producers 1M051, 1M09, 1M10, and 1N06, respectively. Water influx from an aquifer was not included in the model. All four producers were started on production by 1991 by compaction drive. Polymer injection in Well I1 began September 2008. The initial formation pressure was 480 psi. The pore volume compaction coefficient was set to 5.6×10^{-4} psi^{-1}. Many observations and arguments were considered in arriving at this high compressibility value. After considerable deliberation and consideration of (and discarding) alternate production mechanisms (e.g., aquifer drive, gas drive), this high compressibility value was found to provide an acceptable history match of the field performance. Other reservoir properties used in the model are listed in Table 1. Production by compaction occurred between 1991 and 2008 (Year 17). Subsequently, various scenarios were examined involving continued compaction, waterflooding, or polymer flooding using solutions with viscosity from 45 to 205 cp. Our focus was on the case of injecting 125-cp polymer solution. Comparisons were made with compressibility of 1×10^{-6} psi^{-1}. This low compressibility value was chosen to highlight the differences between a nearly incompressible system versus a very compressible system.

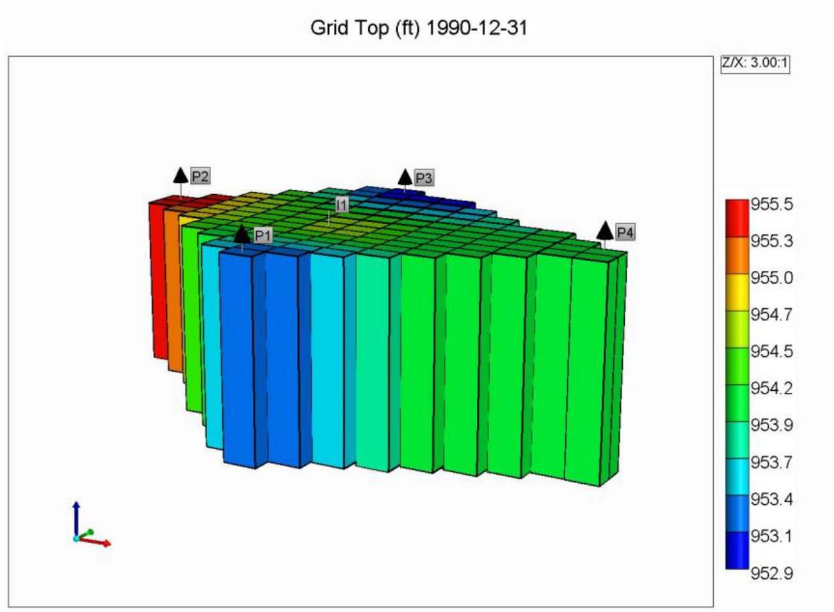

Figure 3—Simulation model

Table 1—Reservoir parameters

Parameters	Average
Initial porosity, fraction	0.338
Initial permeability, md	9917
Swi, %	0.12
Sor,%	0.78
Top depth, ft	953.91
Average net pay, ft	35.71
Initial reservoir pressure, psi	480
Reservoir temperature, °C	38

During the present simulation exercise, some deviations from the actual pilot performance were required to focus on our primary goal (i.e., determining the importance of compressibility on polymer flood performance). The simulations did not stage injection of different polymer viscosities nor did it incorporate staged addition of the two additional patterns to the original pattern. Perhaps, most importantly, a no-flow boundary was imposed surrounding our pattern. Thus, our intent in this paper is not to provide an exact match to the performance of the Sarah Maria polymer flood pilot project.

Overall Pattern Performance

During a 17-year compaction drive with compressibility of 5.6×10^{-4} psi^{-1}, water cut gradually increased to average 20% (consistent with the actual field performance)—compared to 2% if compressibility was 1×10^{-6} psi^{-1}. Oil recovery during this period was 18% OOIP for the high-compressibility case versus 3% OOIP for the low-compressibility case.

Incremental oil recovery from waterflooding and polymer flooding was significantly less after primary production from a compaction drive than when no significant compaction drive occurred—simply because the oil recovery target was less. This point is illustrated in Fig. 4, where for a given circumstance when compressibility was 5.6×10^{-4} psi^{-1}, the incremental oil recovery was roughly half the value for compressibility of 1×10^{-6} psi^{-1}. In particular, after 22 years of 125-cp polymer flooding, cumulative incremental oil production over the compaction drive was 43.9% OOIP with compressibility of 1×10^{-6} psi^{-1} versus 23.6% OOIP with compressibility of 5.6×10^{-4} psi^{-1}. For comparison, after 22 years of waterflooding, cumulative incremental oil production over the compaction drive was 19.7% OOIP with compressibility of 1×10^{-6} psi^{-1} versus 10.7% OOIP with compressibility of 5.6×10^{-4} psi^{-1}. Further, after 22 years of 125-cp polymer flooding, cumulative incremental oil production over waterflooding was 24.2% OOIP with compressibility of 1×10^{-6} psi^{-1} versus 12.9% OOIP with compressibility of 5.6×10^{-4} psi^{-1}. Interestingly, cumulative oil recovery was ultimately 3% OOIP higher with compressibility of 1×10^{-6} psi^{-1} than with 5.6×10^{-4} psi^{-1} (open triangles versus solid triangles in Fig. 4). For the flooding cases, most incremental oil was recovered within five years of starting injection.

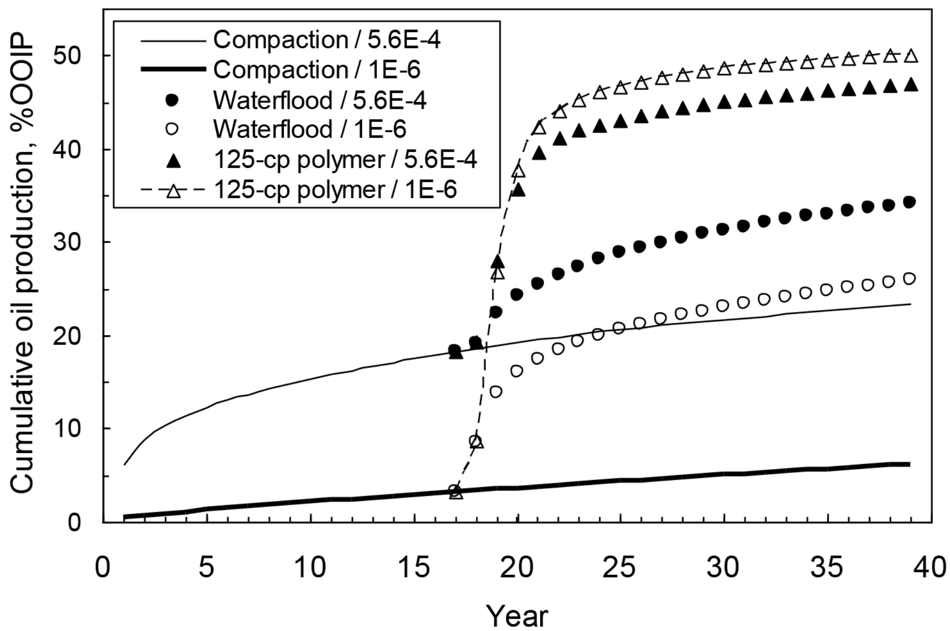

Figure 4—Overall oil production with compressibility = 1×10^{-6} psi^{-1} versus 5.6×10^{-4} psi^{-1}:Compaction, waterflood, and 125-cp polymer flood drives

Fig. 5 provides water cuts associated with the curves in Fig. 4. For primary production with compressibility of 1×10^{-6} psi^{-1}, water cut remained below 5% for the entire 39-year production history (bottom thick curve with no symbols in Fig. 5). In contrast, for primary production with compressibility of 5.6×10^{-4} psi^{-1}, water cut gradually rose to 56% (upper thin curve with no symbols). As explanation for the latter observation, even though the water saturation may have been distributed evenly throughout the reservoir at the time of discovery, water moved preferentially toward production wells during the compaction drive (leaving higher saturations of the viscous oil far from the wells).

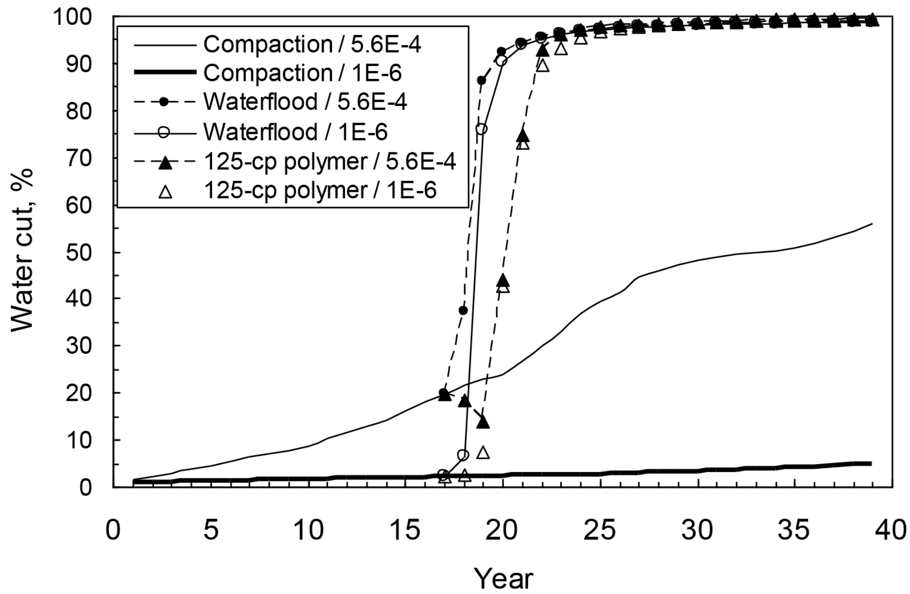

Figure 5—Water cuts associated with Fig. 4

For both compressibility values, water cuts rose to high values within one-year of starting the waterflood (open and solid circles in Fig. 5). They also rose to high values within 3-4 years of starting the 125-cp polymer flood (open and solid triangles in Fig. 5). A modest reduction in water cut (from 20% to 14%) was seen during the first two years of polymer flooding when compressibility was 5.6×10^{-4} psi^{-1}. However, thereafter, the water cuts were very similar for the two compressibility cases.

Performance of Individual Wells

Fig. 6 shows producing water/oil ratios for individual production wells (Wells P1-P4) for compaction drive only, associated with the two compressibility values. For a given compressibility, water cuts showed qualitatively similar behavior (although they increased most for Well P2 and less for Wells P1 and P4). As mentioned above, water cuts remained significantly less for compressibility of 1×10^{-6} psi than for the more compressible case.

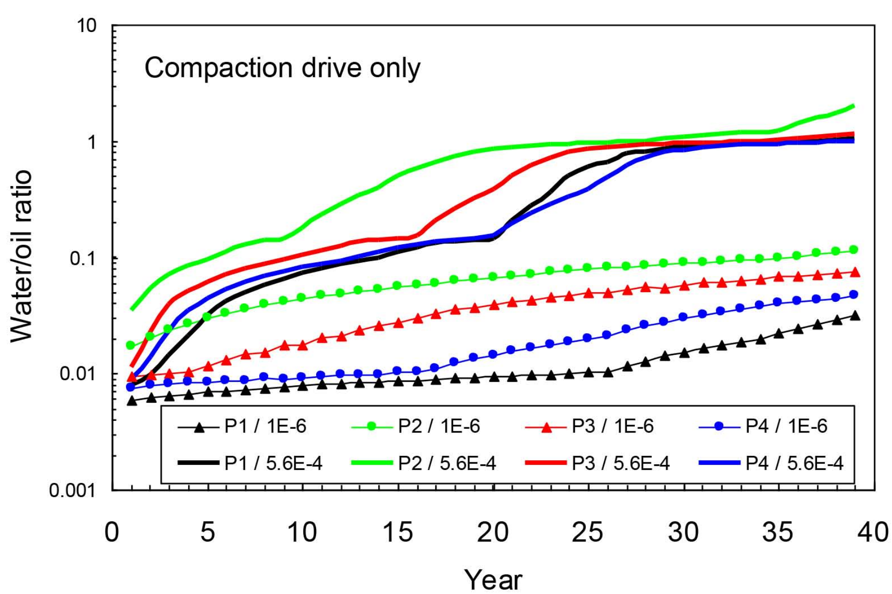

Figure 6—Producing water/oil ratio for compaction drive for individual wells. Legend: P number indicates well. Second number is compressibility in psi^{-1}

Figs. 7 and 8 plot water/oil ratios during waterflooding and 125-cp polymer flooding for the individual wells with the two compressibility values. In Figs. 6-8, water/oil ratios were plotted instead of water cuts to accentuate the differences in response. For the waterflood, in both figures, the water/oil ratio (WOR) increased monotonically with time. With compressibility of 1×10^{-6} psi^{-1}, very small, temporary decreases in WOR were noted in response to the polymer flood (in Wells P2, P3, and P4 in Fig. 7). For compressibility of 5.6×10^{-4} psi^{-1}, more pronounced decreases in WOR were noted in the same wells, in response to the polymer flood (Fig. 8). Presumably, this difference occurred because higher water fractional flows existed at the start of polymer flooding when compressibility was 5.6×10^{-4} psi^{-1}. Well P1 did not exhibit this decrease in WOR for either compressibility—perhaps because resident water saturations were lower in this portion of the pattern. In all cases, WOR values were higher for waterflooding than for polymer flooding during the first 3-6 years of flooding (as expected since the polymer flood provided a more efficient sweep). However, after Year 23, WOR values were less for waterflooding than for polymer flooding because less mobile oil remained in the polymer-swept areas. For both compressibility values, WOR values ultimately were highest in Well P1 (because that was in the most permeable part of the pattern) and lowest in Well P3 (because that was in the least permeable part of the pattern).

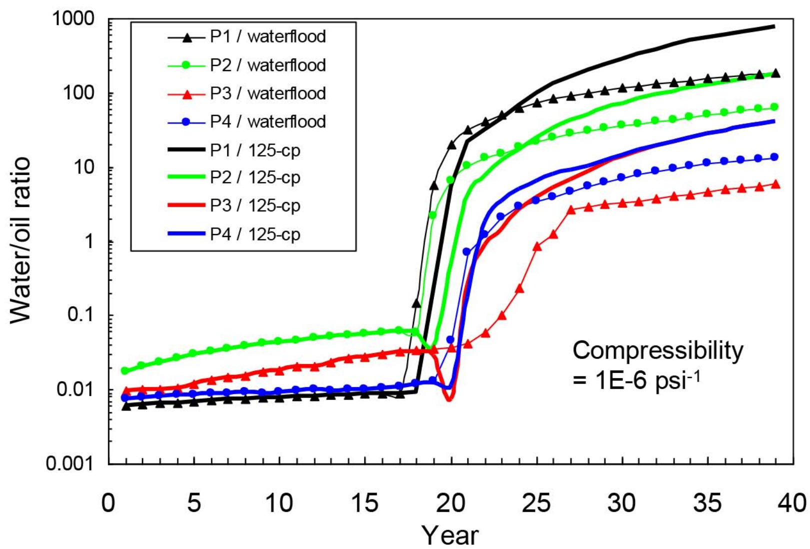

Figure 7—Water/oil ratios for waterflooding and 125-cp polymer flooding with 1 × 10^{-6} psi^{-1} compressibility

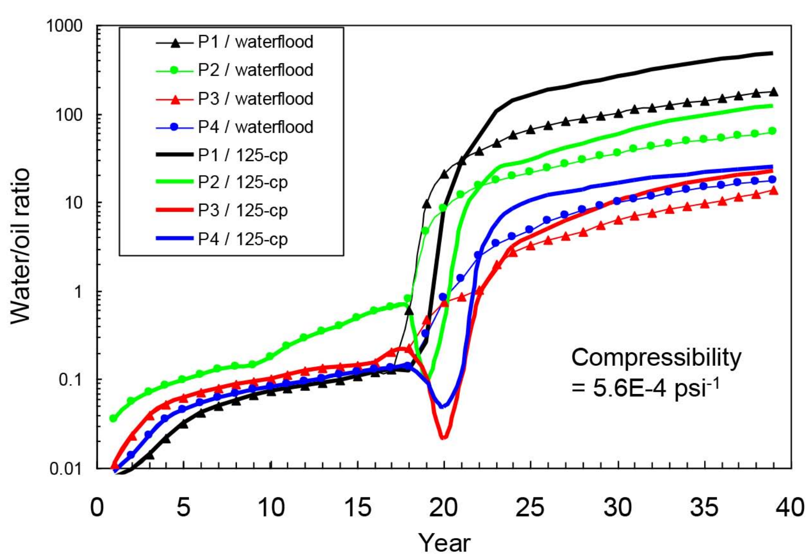

Figure 8—Water/oil ratios for waterflooding and 125-cp polymer flooding with 5.6×10^{-4} psi^{-1} compressibility

Fig. 9 shows incremental oil recoveries for waterflooding over compaction for the individual wells with the two compressibility values. For both compressibility values, Well P1 showed the greatest response, while Well P3 provided the least incremental oil. The positive oil response of Well P1 is consistent the observation that oil saturations were highest in that part of the pattern.

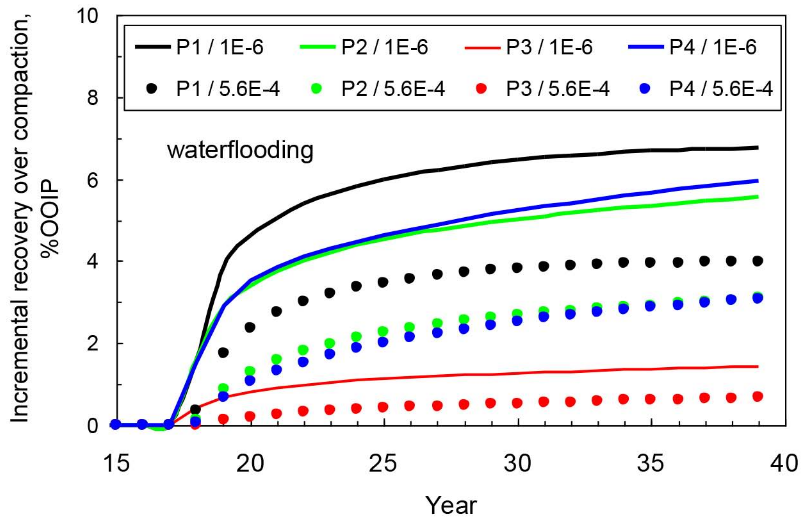

Figure 9—Incremental oil from waterflooding over compaction for individual wells

Fig. 10 shows incremental oil recoveries for 125-cp polymer flooding over compaction for the individual wells with the two compressibility values. In this figure, Well P4 showed the greatest response, while Wells P1 and P3 provided the least incremental oil (for both compressibility values). In comparing Figs. 9 and 10, the polymer flood displaced oil towards Well P4 in preference to Well P1 (relative to the waterflood behavior). From Year 20 onward in Fig. 10, incremental oil (relative to compaction) in Well P1 (black curve and black circles) actually decreased for both compressibility values—again, demonstrating that the polymer pushed oil away from Well P1. This effect was confirmed in the Tambaredjo polymer flood. The well corresponding to Well P1 (1M051) showed a muted response to polymer flooding (Moe Soe Let *et al.* 2012), while the well corresponding to Well P4 (1N06) showed a good response (Delamaide *et al.* 2016).

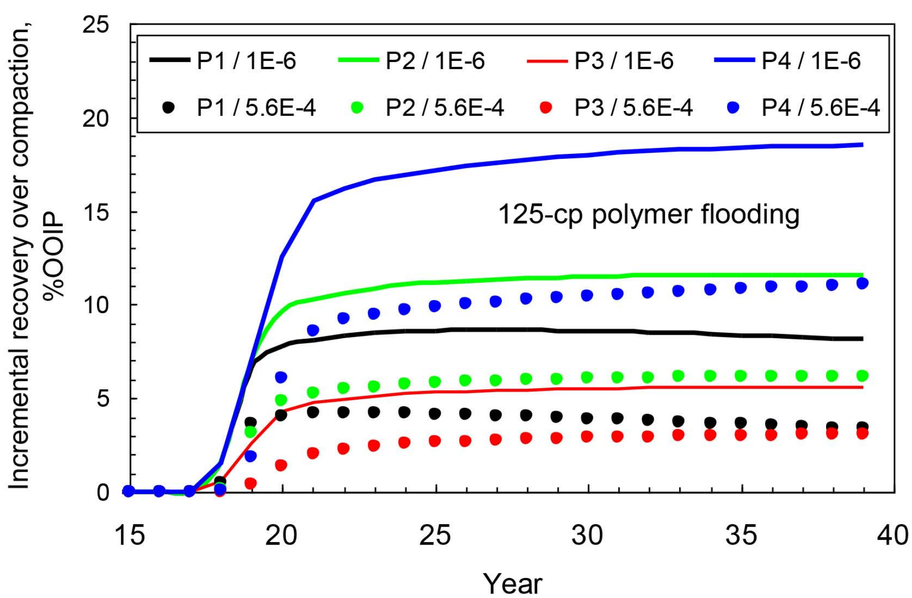

Figure 10—Incremental oil from 125-cp polymer flooding over compaction for individual wells

Fig. 11 shows incremental oil recoveries for 125-cp polymer flooding over waterflooding for the individual wells with the two compressibility values. In this figure, Well P4 showed the greatest response, while Wells P1 and P3 provided the least incremental oil. As mentioned above, the path from the injector toward Well P1 was preferred during waterflooding, but polymer flooding redistributed the pressure gradients and pushed the oil toward Well P4 in preference to Well P1. In later years (Years 30-40) for the high-compressibility case, this effect was great enough to make the cumulative oil production from Well P1 greater during waterflooding than during polymer flooding (solid black circles in Fig. 11).

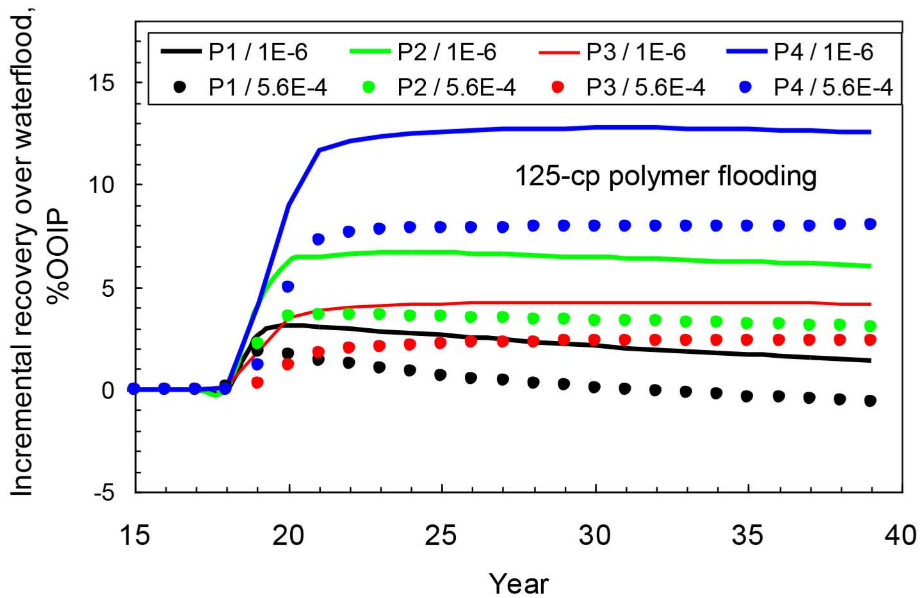

Figure 11—Incremental oil from 125-cp polymer flooding over waterflooding for individual wells

Porosity, Permeability, and Pressure Changes (Compressibility = 5.6×10^{-4} psi^{-1}

Compaction. Fig. 12 plots average porosity for the pattern versus year, while Fig. 13 plots average porosity as a function of oil production volume (in bbl) for the same data. Fig. 14 plots average pattern permeability versus year for the cases of compaction only, 125-cp polymer injection, and re-compaction after 125-cp polymer injection. Fig. 15 plots average reservoir pressure. During the first 17 years of compaction, average porosity in the pattern decreased from an initial value of 0.338 to 0.238—resulting in the production of over 52,000 bbl of oil. Average pattern permeability dropped from 9917 md to 5000 md. Average reservoir pressure decreased from 480 psi initial pressure to 161 psi. Most of these porosity, permeability, and pressure drops occurred during the first five years of compaction.

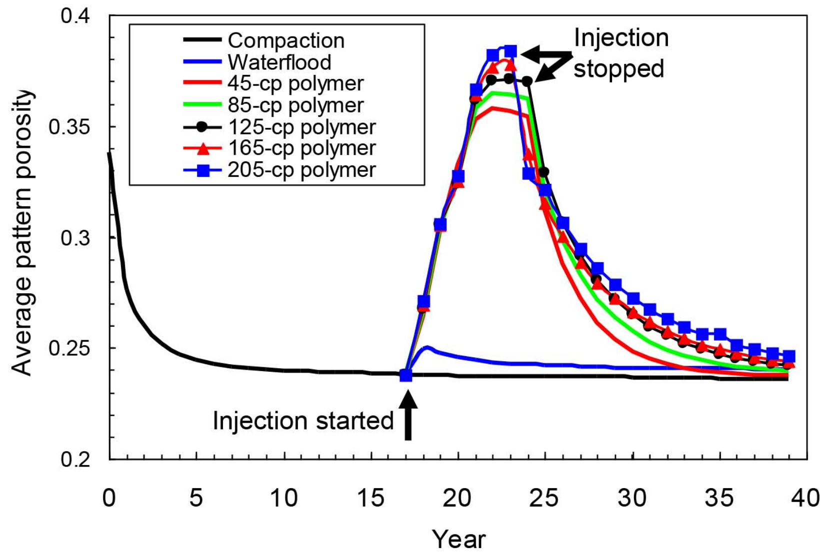

Figure 12—Average porosity for the pattern versus time

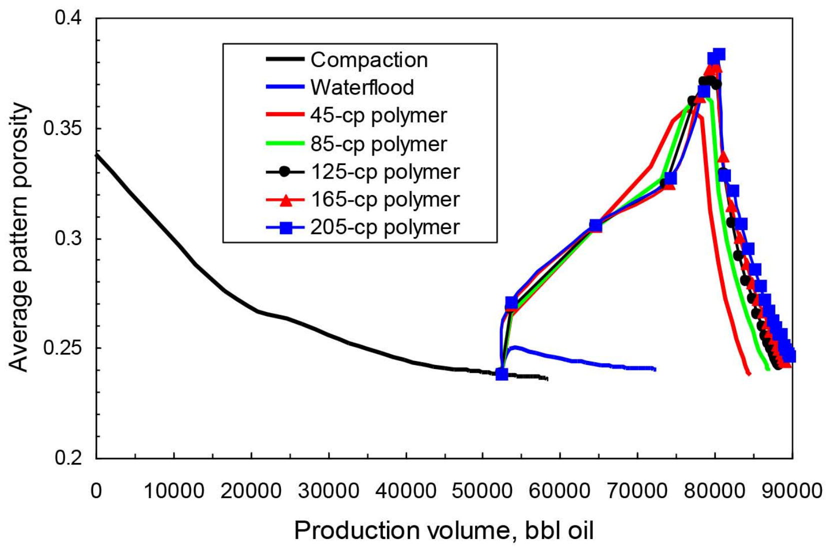

Figure 13—Average porosity for the pattern as a function of cumulative oil production volume

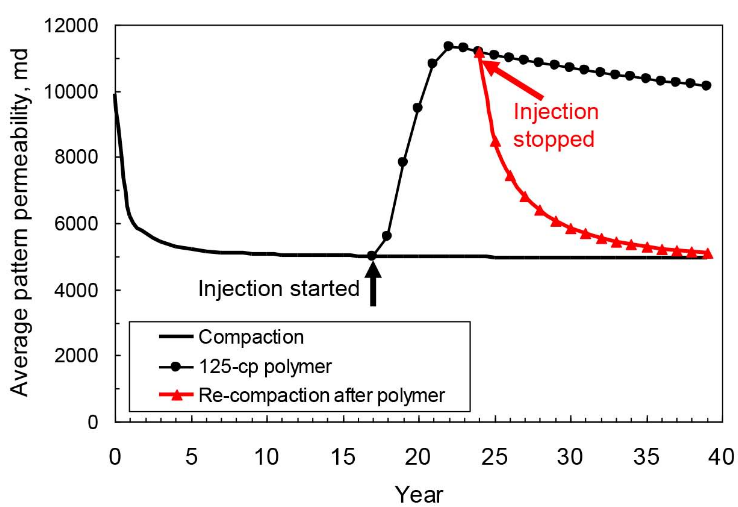

Figure 14—Average permeability for the pattern versus time

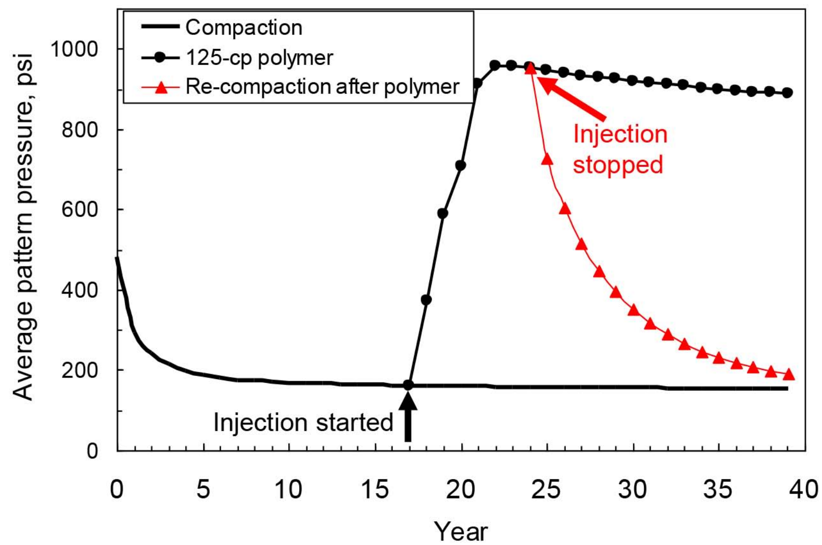

Figure 15—Average pressure for the pattern versus time

Flooding after Compaction. During the first year of waterflooding (Year 18), porosity jumped modestly to 0.25, but then declined thereafter. In contrast, for polymer injection cases, average pattern porosity rose dramatically to 0.36 during the next four years—resulting in the production of an additional 24,000 bbl of oil. Average pattern permeability jumped from 5000 md to 11,300 md. Up to this point, all polymer injection cases followed very similar dilation behavior, regardless of injected polymer viscosity (between 45 cp and 205 cp). Subsequently, the peak in porosity (in Fig. 12) increased modestly with increased injection viscosity: 0.358 for 45 cp, 0.365 for 85 cp, 0.371 for 125 cp, 0.378 for 165 cp, and 0.384 for 205 cp. Average pattern pressure jumped to 958 psi—dangerously close to the overburden pressure. After reaching the peak values, porosity, permeability, and pressure, declined modestly during continued polymer injection (solid circles in Figs. 14 and 15) after the peak in oil production rate (associated with flow of the less mobile polymer solutions that replaced the viscous oil).

Re-Compaction after Polymer Flooding. As mentioned above, most oil recovery occurred within five years after polymer flooding began. The peak in porosity was reached near this time for the highcompressibility cases. For Figs. 4-11 and the solid circles in Figs. 14 and 15, polymer injection was continuous between Year 18 and Year 39. In contrast, for Figs. 12 and 13 and the red curves in Figs. 14 and 15, polymer injection was stopped after reaching the peak in porosity. Thereafter, compaction was allowed to resume. The right side of Fig. 12 reveals that average pattern porosity dropped to 0.24-0.25 by Year 39. During the second compaction period (i.e., post-polymer injection), the additional oil recovery varied from 6150 bbl for 45-cp polymer to 9137 bbl for 205-cp polymer. Thus, a modest level of oil recovery resulted from the second compaction period (25%-38% of the incremental oil during polymer injection), but substantially longer was required for the recovery (15-17 years versus 4-6 years for polymer flooding). Consequently, relying on re-compaction during a period of low oil prices may not be as profitable as one might hope. Average pattern permeability and pressure decreased in conjunction with the porosity decrease (red curves in Figs. 14 and 15).

Pattern-Wide Porosities, Permeabilities, and Pressures (Compressibility = 5.6×10^{-4} psi^{-1})

Fig. 16 shows the distribution of porosities throughout the pattern five years after the start of injecting 125-cp polymer (i.e., at the peak of pattern porosity). For comparison, Fig. 17 shows the distribution of porosities at the same time, assuming that no polymer flood was implemented (i.e., continued compaction). At any given position throughout the pattern, porosity was at least 0.11 units greater during 125-cp polymer injection than for continued compaction. For both polymer injection and continued compaction, the highest porosities were noted in the southern part of the pattern. Since higher permeability is associated with higher porosity, permeabilities (and hence, fluid velocities and oil-recovery values) were highest in the southern part of the pattern. This point is shown in Fig. 18 for 125-cp polymer injection and in Fig. 19 for continued compaction. Consistent with observations from the Tambaredjo polymer flood, substantial variations in performance were noted from well to well—both during the compaction drive and during polymer flooding (Moe Soe Let *et al.* 2012, Delamaide *et al.* 2016). Figs. 16-19 suggest that the variations may be a natural consequence of porosity/permeability variations throughout the field— and not due to the compressible nature of the formation. Although porosity increased by a factor up to 1.5 and permeability increased by a factor up to 2.3, the factor for the increase was fairly uniform throughout the pattern (compare Fig. 16 versus 17 and Fig. 18 versus 19).

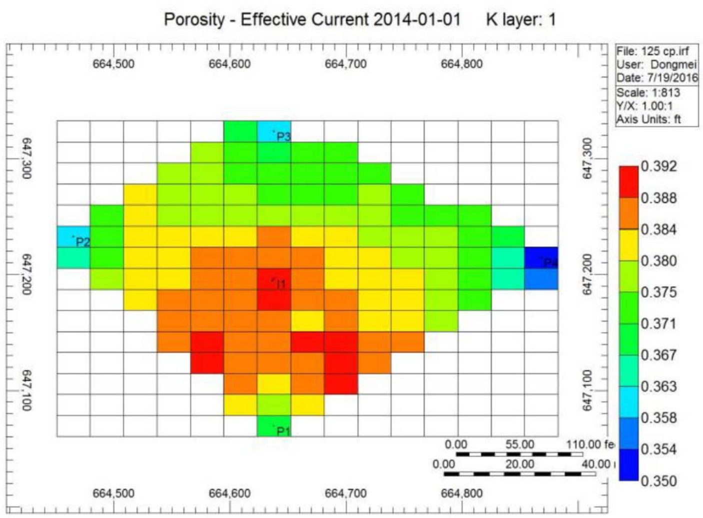

Figure 16—Peak porosities in the pattern, five years after injecting 125-cp polymer

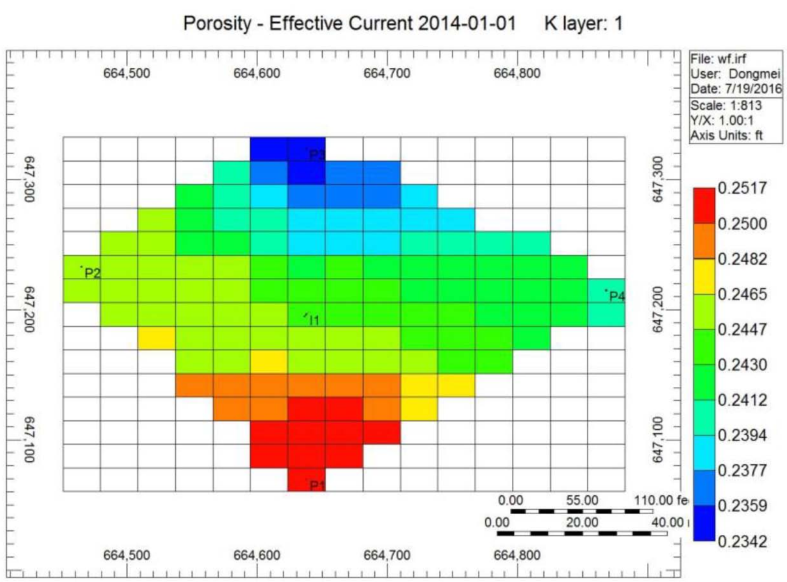

Figure 17—Porosities in the pattern assuming compaction only (at same time as Fig. 16)

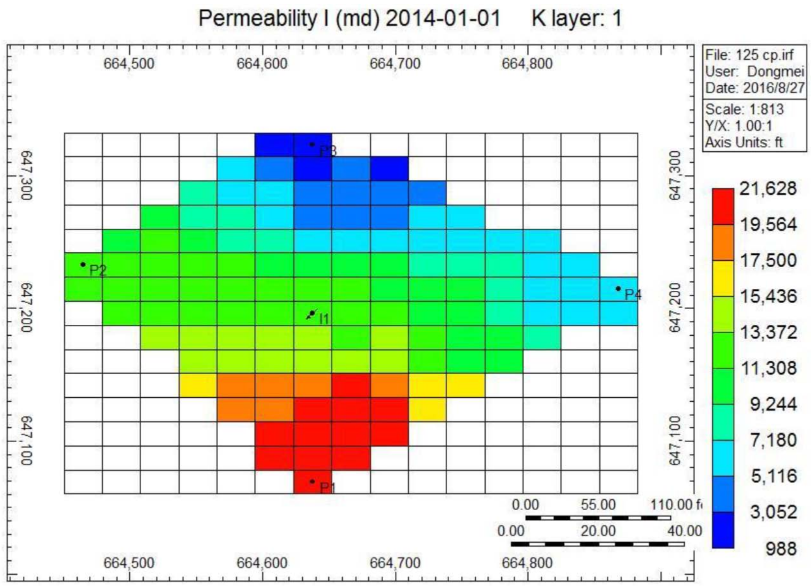

Figure 18—Pattern permeability associated with Fig. 16. 125-cp polymer

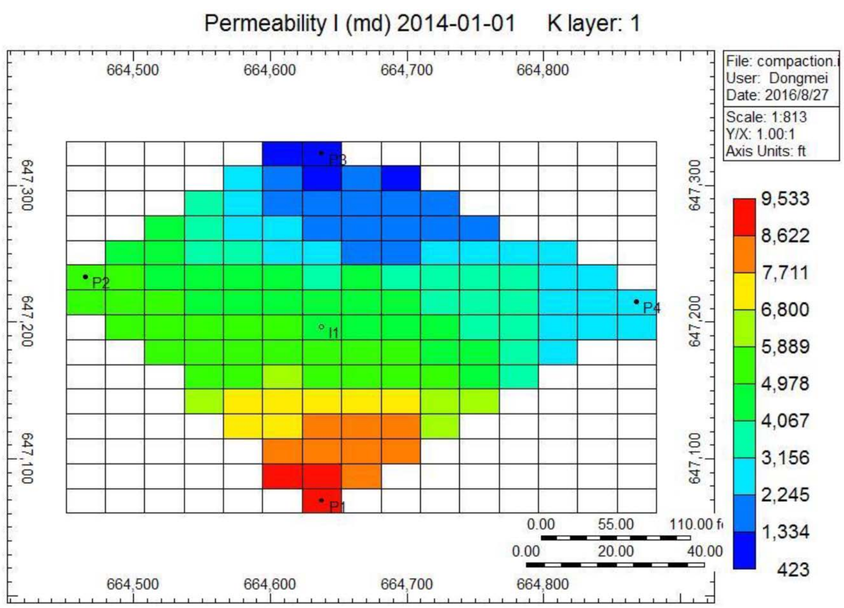

Figure 19—Pattern permeability associated with Fig. 17. Compaction only

Figs. 20 and 21 compare pressures throughout the pattern during polymer injection and continued compaction, respectively. In both cases, pressures were fairly uniform throughout the pattern. Pressures in Fig. 21 were reasonably consistent with pressures observed in the Tambaredjo pilot project before the start of polymer injection in 2008. However, pressures in Fig. 20 (~950 psi) are much higher than actual pilot pressures observed in 2013-2014 (less than 500 psi in shut-in producers). A key reason for the difference is that a no flow boundary was imposed around the pattern during the simulations. In contrast, responses from production wells outside the real pilot project area clearly indicated that a significant volume of the injected polymer flowed outside the pilot area. This information, along with Fig. 20, emphasize the need for maximizing productivity from production wells during polymer floods (whether compressibility is high or not).

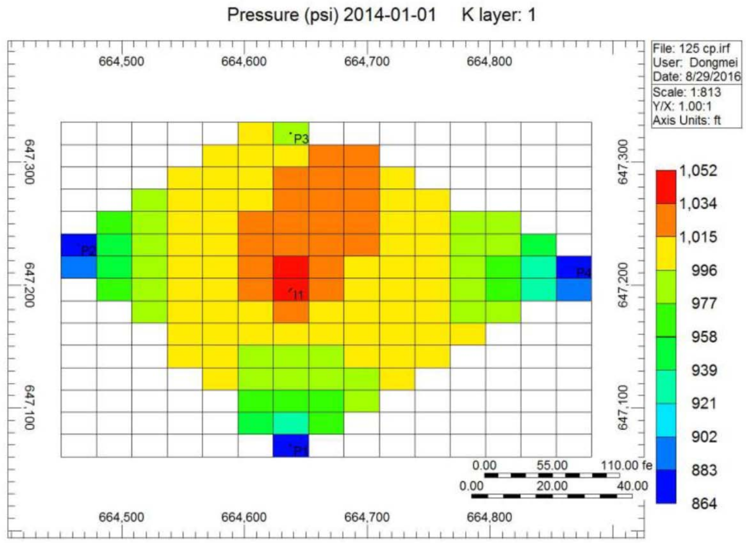

Figure 20—Pattern pressures associated with Fig. 16. 125-cp polymer

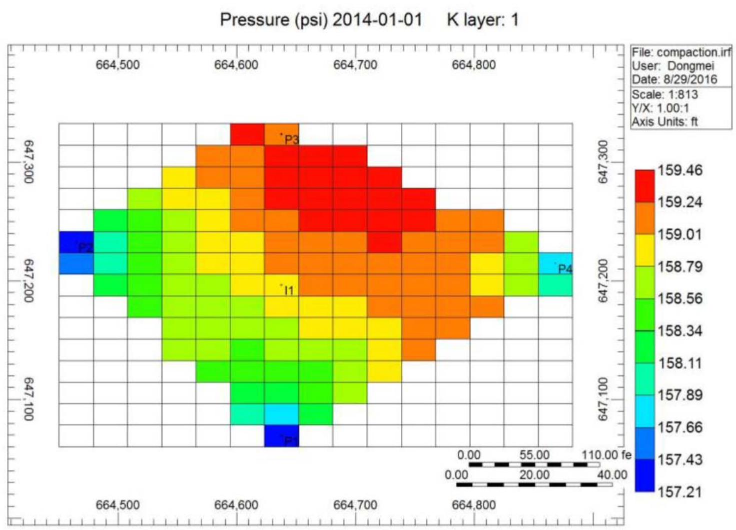

Figure 21—Pattern pressures associated with Fig. 17. Compaction only

Different Voidage Replacement Ratios (VRR)

To this point, the voidage replacement ratio averaged unity during our simulations. (Voidage replacement ratio is the ratio of injected fluid volume to produced fluid volume.) During additional studies, the effect of voidage replacement ratio on flood performance was examined. For cases of waterflooding after compaction, Fig. 22 plots oil recovery versus time for voidage replacement ratios from 0.1 to 10 (in addition to VRR=0 associated with no flood). Figs. 23 to 25 plot similar data for 45-cp, 85-cp, and 125-cp polymer flooding after compaction. Oil recovery increased with increased voidage replacement ratio for waterflooding and generally decreased with increased voidage replacement ratio for polymer flooding.

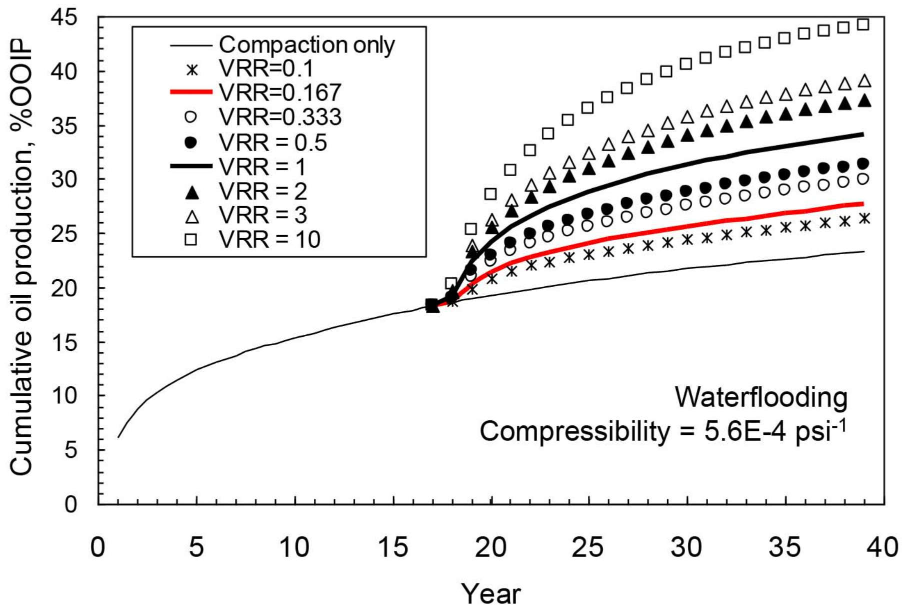

Figure 22—Effect of voidage replacement ratio on waterflooding

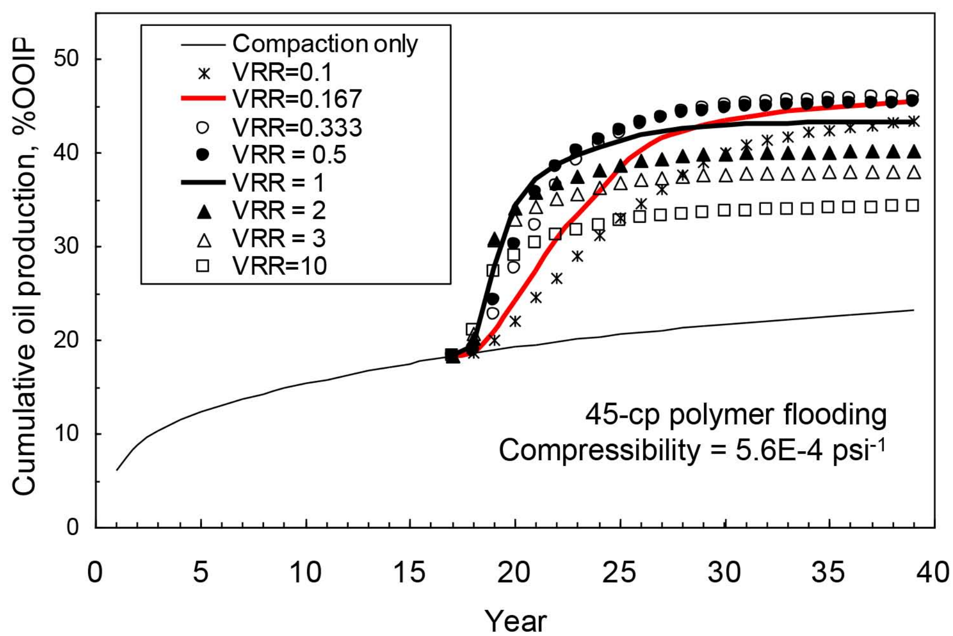

Figure 23—Effect of voidage replacement ratio on 45 cp polymer flooding

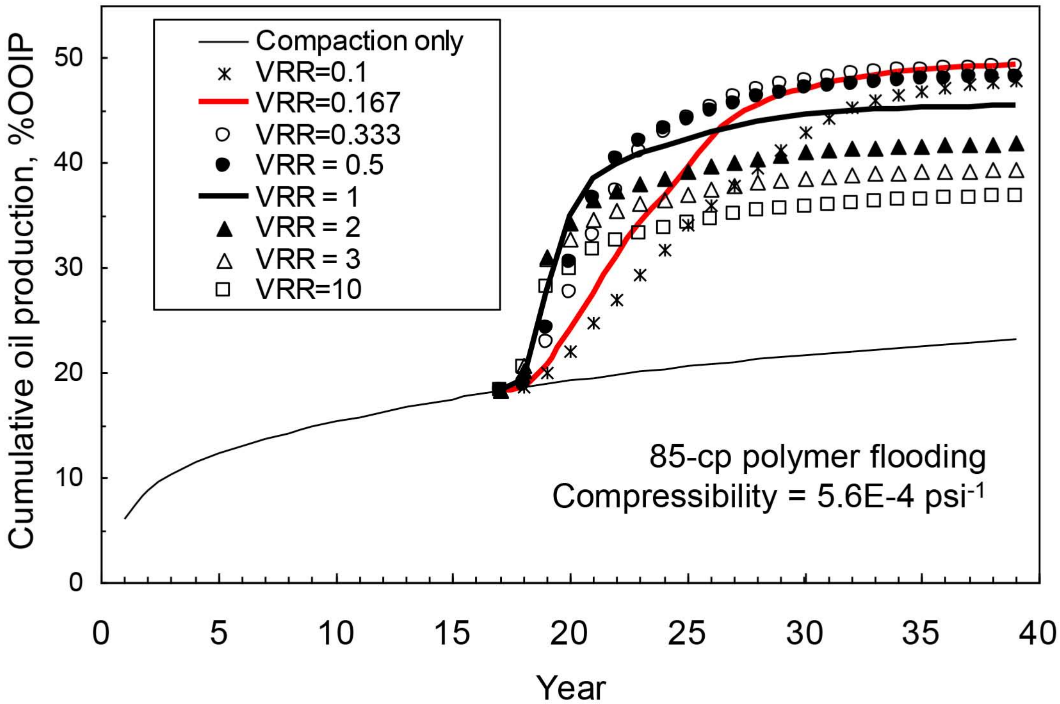

Figure 24—Effect of voidage replacement ratio on 85 cp polymer flooding

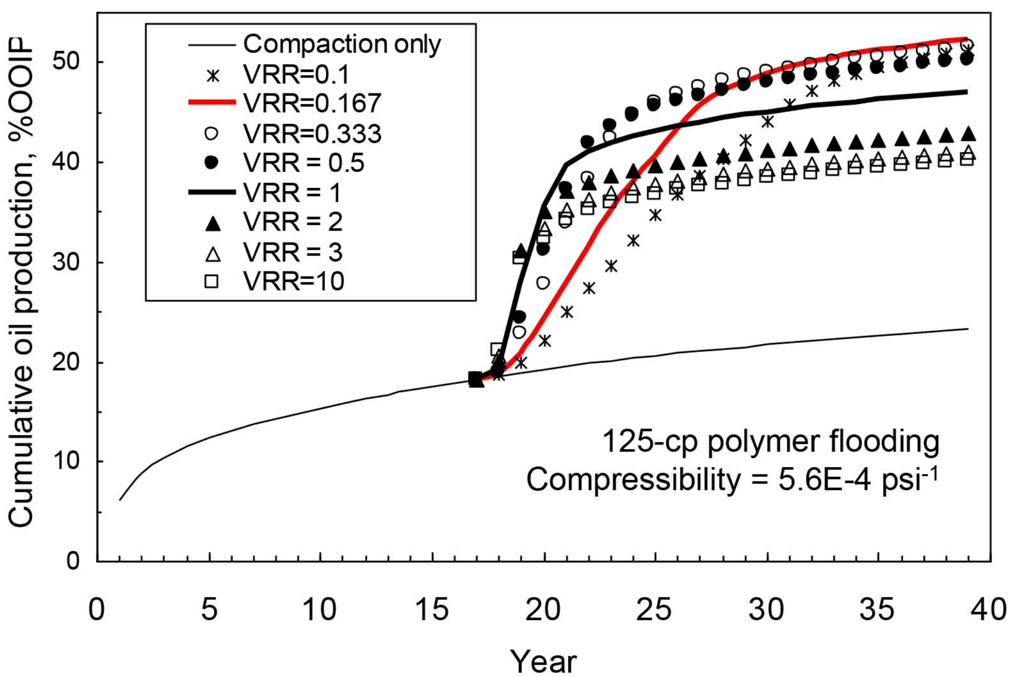

Figure 25—Effect of voidage replacement ratio on 125 cp polymer flooding

To understand the behavior seen in Figs. 22 to 25, Tables 2 and 3 list VRR, peak average pattern porosity, peak average reservoir pressure, and ultimate recovery for waterflooding and polymer floodings with three polymer viscosities. The average pattern porosity for waterflooding did not change much— never exceeding 0.29 even for VRR=10. Thus, little formation dilation was noted during waterflooding. In contrast, during 125-cp polymer flooding, the peak average pattern porosity ranged from 0.265 to 0.437 as VRR ranged from 0.1 to 10. Although ultimate oil recovery (at Year 39) showed a broad maximum for polymer flooding, the oil was recovered most rapidly for VRR values between 0.333 and 0.5 (Fig. 25) and reservoir pressures below 740 psi (Table 2). Ultimate oil recovery from polymer flooding declined for pressures above 740 psi —presumably due to excessive dilation of the reservoir.

Table 2—Ultimate recovery versus VRR and average reservoir pressure By waterflood and 125-cp polymer flood

	Waterflood			125-cp polymer flood		
VRR	Peak φ	Peak ave. reservoir pressure, psi	Oil recovery at Year 39, %OOIP	Peak φ	Peak ave. reservoir pressure, psi	Oil recovery at Year 39, %OOIP
0	0.238	161	23.3	0.238	161	23.3
0.1	0.241	183	26.4	0.265	355	51.3
0.167	0.242	192	27.7	0.281	417	52.2
0.333	0.243	198	29.8	0.308	621	51.5
0.5	0.245	213	31.3	0.329	739	50.2
1	0.248	235	34.1	0.371	954	47.0
2	0.257	298	37.3	0.424	1192	42.9
3	0.263	340	39.1	0.436	1246	41.0
10	0.285	483	44.1	0.437	1372	40.2

Table 3—Ultimate recovery versus VRR and average reservoir pressure By 45-cp, 85-cp polymer floods

	45-cp polymer flood			85-cp polymer flood		
VRR	Peak φ	Peak ave. reservoir pressure, psi	Oil recovery at Year 39, %OOIP	Peak φ	Peak ave. reservoir pressure, psi	Oil recovery at Year 39, %OOIP
0	0.238	161	23.3	0.238	161	23.3
0.1	0.255	287	43.4	0.261	323	47.9
0.167	0.268	372	45.5	0.275	421	49.4
0.333	0.316	547	46.0	0.302	589	49.2
0.5	0.356	664	45.4	0.323	704	48.2
1	0.408	883	43.4	0.365	922	45.5
2	0.443	1126	40.2	0.416	1156	41.9
3	0.462	1270	38.1	0.443	1268	39.4
10	0.255	1345	34.3	0.454	1312	36.9

Note the peak recovery values for each of the four injectant-viscosity cases: 44.1% OOIP for waterflooding VRR=10 (open squares in Fig. 22); 46% OOIP for 45-cp polymer with VRR=0.333 (open circles in Fig. 23); 49.4% OOIP for 85-cp polymer with VRR=0.167 (solid red curve in Fig. 24); and for 125-cp polymer with 52.2% OOIP for 125-cp polymer with VRR=0.167 (solid red curve in Fig. 25). For the case of a waterflood, a very large volume of water (VRR=10) must be injected to achieve the 44.1% OOIP—thus emphasizing our interest in polymer flooding. For the polymer cases, as expected, oil recovery increased with increased injectant viscosity (from 45 to 125 cp), but the peak values were not greatly sensitive to the injected viscosity. Understandably, one may question whether the incremental oil associated with each step up in viscosity was worth the extra polymer cost.

Overall, the most important message from the simulation appears to be that ~500 psi is the optimum average reservoir pressure to target. Note in Tables 2 and 3 that the peak oil recovery values were noted at average reservoir pressures of 483 psi for waterflooding, 547 psi for 45-cp polymer flooding, 421-589 psi for 85-cp polymer flooding, and 417-621 psi for 125-cp polymer flooding.

These results assume a confined pattern and undamaged production wells. For the polymer cases, the results indicate that low VRR ratios are ideal, but that is because the polymer is not flowing outside the pattern during the simulation. In reality (i.e., in the Tambaredjo pilot project), a significant fraction of the polymer is pushing oil toward wells outside the pattern. Hopefully, in an expanded field project, this will be less of an issue.

Of course, the above variations in voidage replacement ratio are directly related to different schemes of injection and production rates. Prior to this work, injecting polymer solutions at the fastest practical rate was believed to be the most profitable course during a polymer flood (Seright 2016). However, Figs. 22 to 25 suggest an optimum rate, viscosity, and pressure for flooding formations where compaction is important. Apparently, for very compressible formations, polymer flooding too rapidly results in pressures that waste much of the injection energy on dilating the formation—thereby detracting from efficient displacement of the oil. Put another way, the responses seen in Figs. 22 to 25 demonstrate a balance between acceleration of oil production by increasing injection rate and injectant viscosity (when comparing waterflooding versus polymer flooding) and production losses caused by dilating the reservoir. For the specific conditions examined here, Tables 2 and 3 suggest that 400-500 psi is the optimum average reservoir pressure to maximize production from this pattern.

Conclusions

The primary goal for this paper was to assess the extent to which the compressible nature of a formation affects polymer flooding. The Tambaredjo field in Suriname (with in-situ oil viscosity ~600 cp) was used as a model for this study. Comparisons were made during simulations where formation compressibility was 5.6×10^{-4} psi^{-1} versus 1×10^{-6} psi^{-1}. The following conclusions were reached during our study:

1. During a 17-year compaction drive with compressibility of 5.6×10^{-4} psi^{-1}, water cut gradually increased to average 20% (consistent with the actual field performance)—compared to 2% if compressibility was 1×10^{-6} psi^{-1}. Oil recovery during this period was 18% OOIP for the highcompressibility case versus 3% OOIP for the low-compressibility case.
2. Subsequent to the above compaction drive, incremental oil recoveries from waterflooding and polymer flooding were significantly less (about half in our case) when compressibility was 5.6×10^{-4} psi^{-1} than when compressibility was 1×10^{-6} psi^{-1}—simply because the oil recovery target was less.
3. For many waterflooding and polymer flooding cases, most incremental oil was recovered within five years of starting injection—regardless of formation compressibility. Water cuts rose to high values within five years of injection, regardless of the viscosity of the injected fluid and the compressibility value.
4. Consistent with the actual field application, the response to polymer injection varied greatly from well to well. However, our analysis indicated that these variations were due to existing heterogeneities within the pattern—not to the high compressibility of the formation. During the simulations, polymer injection increased porosity by factors up to 1.5 and permeability by factors up to 2.3. Nevertheless, compaction or dilation had a fairly even (proportionate) effect on porosity and permeability throughout the pattern.
5. If polymer injection was stopped after the simulated peak in porosity was reached (after 4-6 years of injection) and compaction was allowed to resume, a modest level of oil recovery resulted from this second compaction period (25%-38% of the incremental oil during polymer injection). However, substantially longer was required for the recovery (15-17 years versus 4-6 years for polymer flooding). Consequently, relying on re-compaction during this period of low oil prices may not be as profitable as one might hope.

6. Simulations using various injected polymer viscosities and voidage replacement ratios suggest that there is an optimum rate, viscosity, and pressure for polymer flooding compressible formations. Flooding too rapidly results in pressures that waste much of the injection energy on dilating the formation—thereby detracting from efficient displacement of the oil. These constraints restrict injection rate, viscosity, and pressure to a greater degree for very compressible formations than for incompressible formations.

SI Metric Conversion Factors

cp × 1.0*	E-03 = Pa.s
ft × 3.048*	E-01 = m
md × 9.869 233	E-04 = μm²
psi × 6.894 76	E03 = Pa

*Conversion is exact

Nomenclature

C_p = formation compressibility, psi^{-1}
p = pore pressure, psi
p_{ref} = reference pressure in Eq. 1, psi;
$OOIP$ = original oil in place, %
S_{or} = residual oil saturation, %
S_{wi} = initial water saturation, %
VRR = voidage replacement ratio
φ = porosity, fraction or %
φ_{ref} = reference porosity in Eq. 1, fraction or %

References

Beattie, C. I., Boberg, T. C., & McNab, G. S. 1991. Reservoir Simulation of Cyclic Steam Stimulation in the Cold Lake Oil Sands. *SPE Reservoir Engineering*, May. Society of Petroleum Engineers. SPE18752-PA. http://dx.doi.org/10.2118/18752-PA

CMG STARS Users Guide. 2013. 309.

Cook, C.C. and Jewell, S. 1996. Reservoir Simulation in a North Sea Reservoir Experiencing Significant Compaction Drive. *SPE Res Eng* **11** (1): 48–53. SPE-29132-PA. http://dx.doi.org/10.2118/29132-PA

Delamaide, E., Moe Soe Let, K., Bhoendie, K., Jong-A-Pin, S. and Paidin, W.R. 2016. Results of a Polymer Flooding Pilot in the Tambaredjo Heavy Oil Field, Suriname. Presented at the SPE Canada Heavy Oil Technical Conference. Calgary, Alberta, Canada. 7-9 June. SPE-180739-MS. http://dx.doi.org/10.2118/180739-MS.

Haskell, J.B., Toelsie, S., and Mohan, A. 2010. Optimization of Sand Control for Unconsolidated, Shallow, and Low-pressure Sandstone Reservoirs: A Suriname Case Study. Presented at the Trinidad and Tobago Energy Resources Conference held in Port of Spain, Trinidad. 27-30 June. SPE-133461-MS. http://dx.doi.org/10.2118/133461-MS.

Manichand, R.N., Moe Soe Let, K.P., Gil, L. et al. 2013. Effective Propagation of HPAM Solutions through the Tambaredjo Reservoir during a Polymer Flood. *SPE Prod & Oper* **28** (4): 358–368. SPE-164121-PA. http://dx.doi.org/10.2118/164121-PA.

Manichand, R.N., and Seright, R.S. 2014. Field vs Laboratory Polymer Retention Values for a Polymer Flood in the Tambaredjo Field. *SPE Res Eval & Eng*. **17** (3): 314–325. SPE-169027-PA. http://dx.doi.org/10.2118/169027-PA.

Mayuga, M.N. 1970. Geology and Development of California's Giant—Wilmington Oil Field. Geology of Giant Petroleum Fields, *American Assn. of Petroleum Geologists Memoir* **14**, 158.

Moe Soe Let, K.P., Manichand, R.N., and Seright, R.S. 2012. Polymer Flooding a ~500-cp Oil. Presented at the Eighteenth SPE Improved Oil Recovery Symposium, Tulsa, Oklahoma, USA, 14-18 April 2012. SPE-154567-MS. http://dx.doi.org/10.2118/154567-MS.

Otott, G.E., and Clarke, D.D. 2007. History of the Wilmington Field—1886-1996. AAPG Pacific Section. Old Oil Fields and New Life: A Visit to the Giants of the Los Angeles Basin, 1996. ftp://ftp.conservation.ca.gov/pub/oil/SB4DEIR/docs/CULOtott1996.pdf.

Seright, R.S. 2016. How Much Polymer Should Be Injected During a Polymer Flood? Review of Previous and Current Practices. *SPE J* **21**. SPE179543-PA. http://dx.doi.org/10.2118/179543-PA

Sulak, R.M. 1991. Ekofisk Field: The First 20 Years. *J Pet Technol* **43** (10): 1265–1271. SPE-20773-PA. http://dx.doi.org/10.2118/20773-PA

Sulak, R.M., Thomas, L.K., and Boade, R.R. 1991. 3D Reservoir Simulation of Ekofisk Compaction Drive (includes associated papers 24317 and 24400). *J Pet Technol* **43** (10): 1272–1278. SPE-19802-PA. http://dx.doi.org/10.2118/19802-PA

Yang, Z. et al. 1998. Method of Handling the Complexities Associated with History Matching the Performance of a Highly Stress-sensitive Formation. SPE 49314-MS. http://dx.doi.org/10.2118/49314-MS